OUKA
The University of Osaka
Institutional Knowledge Archive

Title	Enhanced tumor retention of the novel LAT1-targeting PET probe [^{18}F]FAMT-OMe: A comparative study with [^{18}F]FAMT in glioma mouse models
Author(s)	Sampunta, Thosapol; Watabe, Tadashi; Naka, Sadahiro et al.
Citation	Nuclear Medicine and Biology. 2026, 156-157, p. 109623
Version Type	VoR
URL	https://hdl.handle.net/11094/104836
rights	This article is licensed under a Creative Commons Attribution 4.0 International License.
Note	

The University of Osaka Institutional Knowledge Archive : OUKA

https://ir.library.osaka-u.ac.jp/

The University of Osaka

Nuclear Medicine and Biology 156–157 (2026) 109623

Contents lists available at ScienceDirect

Nuclear Medicine and Biology

journal homepage: www.elsevier.com/locate/nucmedbio

Enhanced tumor retention of the novel LAT1-targeting PET probe [^{18}F]FAMT-OMe: A comparative study with [^{18}F]FAMT in glioma mouse models

Thosapol Sampunta [a], Tadashi Watabe [a,b,*], Sadahiro Naka [c], Kazuko Kaneda-Nakashima [b,d], Yoichiro Ohta [e], Takanori Kobayashi [a], Kenta Kurimoto [c], Kayako Isohashi [a], Mitsuaki Tatsumi [f], Hiroki Kato [b], Yoshikatsu Kanai [g], Mitsunori Kirihata [e], Noriyuki Tomiyama [a,b]

[a] Department of Radiology, Graduate School of Medicine, the University of Osaka, Osaka, Japan
[b] Institute for Radiation Sciences, the University of Osaka, Osaka, Japan
[c] Department of Pharmacy, the University of Osaka Hospital, Osaka, Japan
[d] Forefront Research Center, Graduate School of Science, the University of Osaka, Osaka, Japan
[e] Reserch Center for BNCT, Osaka Metropolitan University, Osaka, Japan
[f] Department of Radiology, the University of Osaka Hospital, Osaka, Japan
[g] Department of Bio-system Pharmacology, Graduate School of Medicine, the University of Osaka, Osaka, Japan

ARTICLE INFO

Keywords:
FAMT
LAT1
Oncology
PET
Small animal imaging

ABSTRACT

Introduction: [^{18}F]fluoro-L-α-methyltyrosine ([^{18}F]FAMT) has been reported as a positron-emission tomography (PET) probe that has high specificity for L-type amino acid transporter 1 (LAT1), which is overexpressed in various malignant tumors. However, [^{18}F]FAMT showed rapid washout from the tumor and high retention in the kidney. This study aimed to develop and evaluate a novel LAT1-targeting PET probe, [^{18}F]FAMT-OMe, and compare its performance with [^{18}F]FAMT in glioma xenograft mice.

Methods: [^{18}F]-FAMT-OMe was synthesized via nucleophilic substitution. The uptake of [^{18}F]FAMT-OMe and [^{18}F]FAMT was compared in in vitro studies using C6 glioma and U-87MG cells. PET scans were performed on C6 glioma- and U-87MG tumor-bearing mice (n = 20 each) following intravenous administration of either [^{18}F]FAMT-OMe or [^{18}F]FAMT. After PET/computed tomography (CT) imaging, the organs were weighed and the radioactivity present was measured using a gamma counter.

Results: In vitro analyses demonstrated higher uptake of [^{18}F]FAMT-OMe compared with [^{18}F]FAMT in both C6 and U-87MG cells. PET imaging demonstrated significantly greater tumor retention of [^{18}F]FAMT-OMe than [^{18}F]FAMT (SUVmax at 60 min in C6 glioma: 2.13 ± 0.39 vs. 1.09 ± 0.79, $P < 0.05$). The kidneys and urine showed significantly lower uptake and excretion of [^{18}F]FAMT-OMe than [^{18}F]FAMT (kidney uptake: SUVmean 3.75 ± 0.89 vs. 5.55 ± 2.44, $P < 0.05$ urine excretion: SUVmean 16.50 ± 7.65 vs. 34.38 ± 8.74, $P < 0.05$), while blood retention of [^{18}F]FAMT-OMe was significantly increased (SUVmean 1.78 ± 0.85 vs. 1.20 ± 0.82, $P < 0.05$).

Conclusion: [^{18}F]FAMT-OMe showed improved tumor retention on PET compared with [^{18}F]FAMT in the C6 glioma tumor model, suggesting its potential utility for future applications in LAT1-targeted PET.

1. Introduction

[^{18}F]-fluorodeoxyglucose ([^{18}F]FDG) is the most widely used positron-emission tomography (PET) probe for assessing various malignant tumors. However, [^{18}F]FDG has some limitations, such as inflammatory uptake in benign lesions, which yields some false-positive results in malignant tumors [1]. [^{18}F]-3-fluoro-L-α-methyl-tyrosine ([^{18}F]FAMT) is a radio-labeled amino acid PET probe with high specificity for L-type amino acid transporter 1 (LAT1, SLC7A5) [2]. LAT1 is overexpressed in many types of cancer cells—it regulates the transport of several neutral amino acids, such as phenylalanine, leucine, isoleucine, tryptophan, histidine, and tyrosine, promoting cancer cell growth

* Corresponding author at: Department of Radiology, Graduate School of Medicine, the University of Osaka, 2-2 Yamadaoka, Suita, Osaka, 565-0871, Japan.
E-mail address: watabe.tadashi.med@osaka-u.ac.jp (T. Watabe).

https://doi.org/10.1016/j.nucmedbio.2026.109623
Received 30 November 2025; Received in revised form 25 February 2026; Accepted 9 March 2026
Available online 13 March 2026
0969-8051/© 2026 The Author(s). Published by Elsevier Inc. This is an open access article under the CC BY license (http://creativecommons.org/licenses/by/4.0/).

[2,3]. In contrast, LAT1 expression is minimal in healthy organs, leading to a low physiological accumulation of LAT1-targeting PET probes [4]. Several studies have shown that the chemical structure of [^{18}F]FAMT has a high specificity for LAT1, particularly in the presence of an alpha-methyl moiety. Therefore, [^{18}F]FAMT is a promising PET probe for tumor-specific diagnostic imaging [2,4,5].

However, [^{18}F]FAMT has been reported to accumulate in the renal tubular epithelial cells through the organic anion transporter 1 (OAT1) [5]. Probenecid, furosemide, and ethacrynic acid can reduce the high renal accumulation of FAMT by suppressing the uptake of the radiotracer into renal tubular epithelial through OAT1 [6,7]. A previous study also reported that the tumor uptake of 3-^{125}I-L-α-methyl-tyrosine ([^{125}I]IMT), which has a chemical amino acid structure similar to that of FAMT, can be enhanced by administering probenecid, via suppression of the interaction of OAT1 and [^{125}I]IMT in mouse kidneys [8]. Recently, a study reported that the hydroxyl group (-OH) of [^{18}F]FAMT is responsible for its transport by OAT1 in the kidney [5]. Therefore, [^{18}F]FAMT-OMe, in which the hydroxyl group is substituted with a methoxy group (-O-CH_3), is expected to interact less with OAT1 than [^{18}F]FAMT.

This study investigated the biodistribution and tumor uptake of this novel PET probe, [^{18}F]FAMT-OMe, in glioma xenograft mice, as compared with that of [^{18}F]FAMT.

2. Materials and methods

2.1. Synthesis of [^{18}F]FAMT and [^{18}F]FAMT-OMe

A novel precursor with pinacolborate introduced at the 3-position of the benzene ring for direct radiolabeling with [^{18}F]fluoride was used. The synthesis procedures for [^{18}F]FAMT and [^{18}F]FAMT-OMe are briefly described in Fig. 1. The synthesis of the precursor and the standard for [^{18}F]FAMT-OMe and [^{18}F]FAMT are also described in Supplementary Data (Supplementary Figs. S1–S2). [^{18}F]fluoride was trapped on an anion-exchange cartridge (QMA carbonate, 46 mg sorbent) and eluted into the reactor (10-mL glass vial) by 0.5 mL of a TEA-HCO_3/methanol solution (5.4 mg/mL). The eluate was evaporated, after which 1 mL of the precursor solution (17 μmol of precursor and 61–63 μmol of $Cu(OTf)_2(Py)_4$, as a catalyst, in *N*,*N*-dimethylacetamide) was added. The fluorination conditions were set to 110 °C for 20 min, with stirring. To the reaction mixture, 2 mL of ethanol was added. The solution was passed through a 1-g silica column and then passed through an additional 3 mL of ethanol to remove the copper ions. All the solutions that passed through the silica column were collected in another reactor. After evaporation of the solvent, the fluorinated products were deprotected with 1 mL of 2 M HCl (12 M HCl was used for the first batch only) at 95 °C for 10 min for [^{18}F]FAMT-OMe, and with 0.5 mL of 57% HI at 120 °C for 20 min for [^{18}F]FAMT. Approximately 2 mL of the reaction solution was prepared by adding water for injection (WFI), and [^{18}F]FAMT-OMe and [^{18}F]FAMT were separated using preparative high-performance liquid chromatography (HPLC). In the HPLC column, a YMC Pack ODS AQ 250 × 10 mm (YMC, Kyoto, Japan) was used for both [^{18}F]FAMT-OMe and [^{18}F]FAMT. As eluent, 0.1% acetic acid/ethanol = 90/10 (0.1% acetic acid/methanol = 80/20 was used for the first batch only) was used for [^{18}F]FAMT-OMe, while 0.1% acetic acid/ethanol = 95/5 was used for [^{18}F]FAMT. The flow rate was set to 4 mL/min and [^{18}F]FAMT-OMe and [^{18}F]FAMT were detected using UV (wavelength 280 nm) and a radioactivity detector. The HPLC fraction was prepared at pH 5–6 with 25% ascorbic acid injection or 7% sodium bicarbonate injection and was used directly or diluted with WFI.

2.2. Cell culture

C6 glioma and U-87MG cell lines were obtained from the RIKEN Cell Bank (Tsukuba, Japan). The C6 glioma cell line was cultured in RPMI-1640 with L-Glutamine and Phenol Red (FUJIFILM Wako Pure Chemical Corporation, Osaka, Japan), while the U-87MG cell line was cultured in Dulbecco's modified Eagle medium (D-MEM, High Glucose) with L-Glutamine and Phenol Red (FUJIFILM Wako Pure Chemical Corporation, Osaka, Japan), containing 10% heat-inactivated fetal bovine serum (Corning Life Science, Woodland, Canada) and 1% penicillin–streptomycin (FUJIFILM Wako Pure Chemical). The cells were cultured in sterile 100-mm tissue culture dishes (IWAKI AGC Techno Glass CO., LTD, Shizuoka, Japan) in a CO_2 incubator (AS ONE INCUBATOR E-50, QTE Technologies, Hanoi, Vietnam) under 5.0% CO_2 and at 37 °C. Cultured cells were counted using a TC20™ Automated Cell Counter (Bio-Rad, Osaka, Japan).

2.3. In vitro cellular uptake analysis

C6 glioma and U-87MG cells were seeded in 24-well cell culture plates at a density of 1 × 10^5 cells/mL. Two days later, the cells were washed with phosphate-buffered saline (PBS) and the culture medium

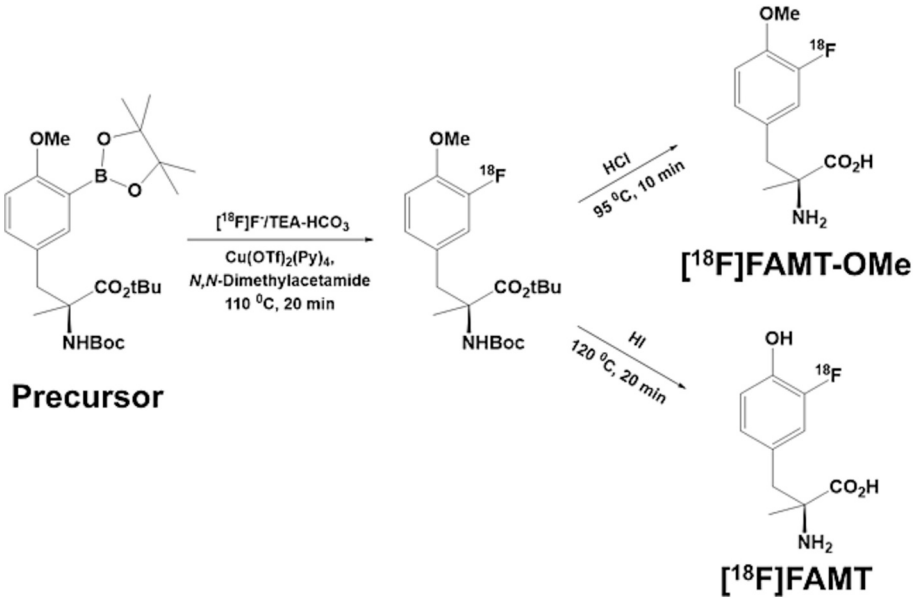

Fig. 1. Schematic of the synthesis of [^{18}F]FAMT-OMe and [^{18}F]FAMT.

was replaced with Hanks' balanced salt solution buffer. After the addition of [^{18}F]FAMT or [^{18}F]FAMT-OMe, cells were collected at 0.5, 1, 5, and 10 min. Cells were washed with PBS (−) three times and then lysed with 0.1 N NaOH solution. The cell lysates were analyzed using a BeWell QS-02 well-type gamma counter (Molecular Imaging Laboratory, Inc., Osaka, Japan). Protein amounts were measured and the uptake amounts were corrected based on the number of cells.

For LAT1 blocking study, HEK293, LAT1/HEK293 (were established and provided by Dr. Kanai [9]), C6 glioma, and U-87MG cells were seeded in 24-well cell culture plates at a density of 1×10^5 cells/mL. After the addition of 20 mM 2-aminobicyclo[2.2.1]heptane-2-carboxylic acid (BCH) (Sigma-Aldrich, St. Louis, MO, USA) or 10 μM O-[(5-amino-2-phenyl-7-benzoxazolyl)methyl]-3,5-dichloro-L-tyrosine (Nanvuranlat) (Cayman Chemical, Ann Arbor, MI, USA), uptake was measured at 0.5, 5, and 10 min.

2.4. Preparation of animals

This study was performed in compliance with the guidelines of the Institute of Experimental Animal Sciences. The protocol was approved by the Animal Care and Use Committee of Osaka University Graduate School of Medicine. Seven-week-old male BALB/c nude mice ($n = 40$, body weight 25.3 ± 2.8 g) were purchased from Japan SLC, Inc. (Shizuoka, Japan). The mice were housed under a 12-h light/12-h dark cycle, with free access to food and water. After 1 week of acclimatization, tumor cells, suspended in a 1:1 mixture of culture medium and Matrigel (Corning Life Science, Tewksbury, MA, USA), were subcutaneously implanted (approximately 1×10^7 cells) into nude mice (C6 glioma model: $n = 20$ mice; U-87MG model: n = 20 mice). Antibiotics (10 mg/kg, Baytril® 5% w/v, Bayer HealthCare, Tokyo, Japan) were also administered after the tumor cell inoculation. The mice were monitored and their body weights and tumor sizes were measured periodically.

2.5. PET static and dynamic acquisitions

Three weeks after tumor transplantation, PET images were acquired under isoflurane inhalation anesthesia. [^{18}F]FAMT-OMe (11.62 ± 1.57 MBq) or [^{18}F]FAMT (12.76 ± 5.24 MBq) were intravenously injected into the C6 glioma xenograft mice ($n = 6$ and $n = 5$, respectively) and U-87MG xenograft mice (n = 6 and n = 6, respectively) (Table 1). A 10-min static PET/CT acquisition was performed using a micro PET/CT scanner (SIEMENS Inveon, Munich, Germany) 60 min after PET probe injection ($n = 23$). A 60-min PET/CT dynamic acquisition was also performed immediately following the PET probe injection in selected subjects ($n = 10$) (Table 1). PET images were reconstructed using the ordered subsets expectation-maximization 3-dimensional iterative/maximum a posteriori method (OSEM3D/SP-MAP) with a matrix size of 128 × 128. The OSEM3D/SP-MAP parameters were set to two OSEM iterations, 18 MAP iterations, and a target resolution of 1.5 mm. CT images were reconstructed using the Feldkamp algorithm with four iterations, Shepp-Logan filter, and beam-hardening correction.

Table 1
Number of mice in each group for positron-emission tomography PET imaging analysis and biodistribution.

	C6 glioma (n = 20)		U-87MG (n = 20)	
	[^{18}]F-FAMT-OMe (n = 10)	[^{18}]F-FAMT (n = 10)	[^{18}]F-FAMT-OMe (n = 11)	[^{18}]F-FAMT (n = 9)
PET acquisition	(Total) n = 6	(Total) n = 5	(Total) n = 6	(Total) n = 6
Dynamic PET	n = 3	n = 2	n = 3	n = 2
Static PET	n = 3	n = 3	n = 3	n = 4
Biodistribution	(Total) n = 10	(Total) n = 10	(Total) n = 11	(Total) n = 9
With PET acquisition	n = 6	n = 5	n = 6	n = 6
Without PET acquisition	n = 4	n = 5	n = 5	n = 3

For in vivo blocking study, [^{18}F]FAMT-OMe (12.73 ± 1.17 MBq), followed by 20 mM BCH (n = 3) or 10 μM Nanvuranlat (n = 3), was intravenously injected into the C6 glioma xenograft mice. A 60-min PET/CT dynamic acquisition was also performed immediately following the LAT1 inhibitor and PET probe injection.

2.6. PET imaging analysis

PET images were analyzed using PMOD 4.0 software (PMOD Technologies LLC, Fällanden, Switzerland). Volumes of interest (VOIs) were drawn around the organs of interest using sphere tool as the analytic object for standardized uptake value (SUV) measurements. Isocontouring was performed by setting a threshold of 50% of SUVmax in the VOI for measuring the average, minimum, and maximum SUV values in the enclosed VOI. The SUVmean and SUVmax of tumors and healthy organs were compared between [^{18}F]FAMT-OMe and [^{18}F]FAMT PET.

2.7. Measurement by gamma counter

All mice were sacrificed and dissected for organ collection after PET/CT. The mice were euthanized by overdose isoflurane anesthesia after PET acquisition. Additional mice evaluated solely for biodistribution were also included ($n = 17$). Blood and urine samples were collected immediately after euthanasia, using a 29-gauge needle syringe. The tumor, brain, submandibular glands, heart, lungs, liver, pancreas, spleen, kidneys, testes, epididymis, and spine (Cervical spine (C1) – Lumbar spine (L6)) were collected, and the weight of each organ was measured using a GR-60 Semi-Micro Balance (A&D, Tokyo, Japan) and a BeWell QS-02 gamma counter (Molecular Imaging Laboratories).

2.8. Statistical analysis

Comparisons between two groups were performed using a two-tailed *t*-test in SPSS (version 25.0, IBM Corp., Armonk, NY, USA), with a significance level set at $P < 0.05$. The quantitative results of this study were represented as mean ± SD.

3. Results

The synthesis results of the precursor and reference standard for [^{18}F]FAMT-OMe and [^{18}F]FAMT are shown in the Supplementary Data. Using the starting activity of ^{18}F as 37 to 66 GBq, [^{18}F]FAMT-OMe and [^{18}F]FAMT were obtained with radioactivity of 3324 ± 879 MBq and 2173 ± 720 MBq at 94 ± 5 min and 102 ± 2 min, their radiochemical yields were 11 ± 3% and 11 ± 4%, respectively at the end of synthesis. The radiochemical purity exceeded 99%, and the molar activity were 835 ± 193 GBq/μmol and 518 ± 61 GBq/μmol respectively. The enantiomeric purities of [^{18}F]FAMT-OMe and [^{18}F]FAMT were over 90% for the ^{18}F-L-form. The HPLC chromatograms of [^{18}F]FAMT-OMe and [^{18}F]FAMT are shown in the Supplementary Data (Supplementary Figs. S3–S6).

The in vitro uptake experiment using C6 glioma and U-87MG cells is shown in Fig. 2a. [^{18}F]FAMT-OMe uptake was significantly higher than that of [^{18}F]FAMT at almost time points in both C6 glioma and U-87MG tumor cells. The in vitro uptake in blocking experiment using HEK293 and LAT1/HEK293 cells is shown in Fig. 2b and c. After treatment with BCH or Nanvuranlat, [^{18}F]FAMT-OMe uptake was significantly inhibited in LAT1/HEK293, C6 glioma and U-87MG cells compared with the control group at all time points ($P < 0.05$).

Representative PET/CT images at 60-min post-injection are shown in Fig. 3. [^{18}F]FAMT-OMe PET showed higher uptake than that of [^{18}F]FAMT PET in both C6 glioma and U-87MG xenograft mice based on

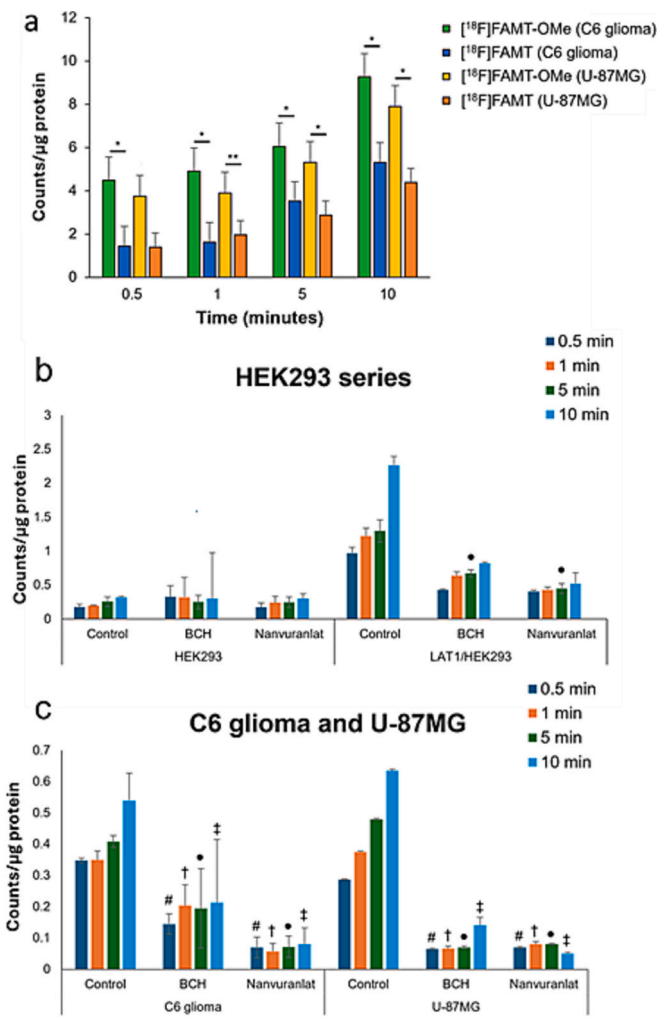

Fig. 2. (a) In vitro cellular uptake analysis of [^{18}F]FAMT-OMe and [^{18}F]FAMT using C6 glioma and U-87MG cells (*$P < 0.05$, **$P < 0.01$). (b) In vitro blocking study of [^{18}F]FAMT-OMe using HEK293 and LAT1/HEK293 cells with BCH or Nanvuranlat. (c) In vitro blocking study of [^{18}F]FAMT-OMe using C6 glioma and U-87MG cells with BCH or Nanvuranlat. Symbols (#, †, ●, ‡) indicate significant differences at 0.5, 1, 5, and 10 min, respectively, compared with each control group ($P < 0.05$).

visual evaluation. The SUVmax and SUVmean of [^{18}F]FAMT-OMe in C6 glioma ($n = 6$) were significantly higher than those of [^{18}F]FAMT ($n = 5$) (SUVmax: 2.13 ± 0.39 vs. 1.09 ± 0.79, SUVmean: 1.48 ± 0.26 vs.0.78 ± 0.57, respectively) ($P < 0.05$) (Fig. 4a, b). In U-87MG tumor, SUVmax and SUVmean of [^{18}F]FAMT-OMe (n = 6) showed higher uptake than [^{18}F]FAMT (n = 6), although the difference did not reach statistical significance (SUVmax: 1.26 ± 0.26 vs.1.04 ± 0.33, respectively) ($P = 0.23$) (SUVmean: 0.86 ± 0.10 vs.0.72 ± 0.22, respectively) ($P = 0.19$). As shown in Fig. 4c, the SUVmean of [^{18}F]FAMT-OMe in the kidney and urine was significantly lower than that of [^{18}F]FAMT (3.75 ± 0.89 vs. 5.55 ± 2.44 and 16.50 ± 7.65 vs. 34.38 ± 8.74, respectively) ($P < 0.05$). The SUVmean of the brain, submandibular glands, lungs, heart, liver, pancreas, spleen, spine, testes, and epididymis of [^{18}F]FAMT-OMe was significantly higher than that of [^{18}F]FAMT ($P < 0.05$).

The biodistribution determined by using a gamma counter is shown in Fig. 5. For C6 glioma tumors, the %ID/g of [^{18}F]FAMT-OMe ($n = 10$) was significantly higher than that of [^{18}F]FAMT (n = 10) (4.49 ± 3.07 vs. 1.83 ± 1.44, respectively) (P < 0.05) (Fig. 5a). The %ID/g of [^{18}F]FAMT-OMe in the kidney was significantly lower than that of [^{18}F]FAMT (10.85 ± 3.45 and 15.00 ± 5.01, respectively) ($P < 0.01$). The %ID/g of [^{18}F]FAMT-OMe was also significantly higher than that of [^{18}F]FAMT in the blood and spine (blood: 1.78 ± 0.85 and 1.20 ± 0.82, spine: 1.52 ± 0.52 and 1.04 ± 0.41, respectively) (P < 0.05) (Fig. 5b).

For C6 glioma tumors, the dynamic PET curve showed a higher SUVmean for [^{18}F]FAMT-OMe than that for [^{18}F]FAMT until 60 min after administration (Fig. 6a). The dynamic PET curve of [^{18}F]FAMT-OMe remained stable as compared to that of [^{18}F]FAMT, with washout kinetics in the U-87MG tumor xenograft model (Fig. 6b). Dynamic PET revealed that the renal uptake and urine excretion of [^{18}F]FAMT-OMe was lower than that of [^{18}F]FAMT (Fig. 6c and h). In contrast, a higher uptake of [^{18}F]FAMT-OMe was observed in the brain, submandibular glands, lungs, heart, liver, pancreas, spleen, testes, epididymis, spine, and blood compared with [^{18}F]FAMT (Fig. 6d–g and Supplementary Fig. S7).

Representative PET/CT images of [^{18}F]FAMT-OMe in C6 glioma xenograft mice pretreated with BCH or Nanvuranlat and control group are shown in Fig. 7a. The dynamic curves were clearly lower in the BCH- ($n = 3$) and Nanvuranlat-pretreated groups (n = 3) compared to those in control group (n = 3) in Fig. 7b. Comparisons of SUVmean and %ID/g in static PET images at 60 min post-injection are shown in Fig. 7c and d. Although these differences did not reach statistical significance, there was a trend toward decreased accumulation in the BCH- and Nanvuranlat-pretreated groups compared with the control group, suggesting that LAT1 inhibition reduces tracer accumulation.

4. Discussion

In this study, we confirmed the high retention of [^{18}F]FAMT-OMe in glioma tumors compared with [^{18}F]FAMT, along with reduced renal uptake and urinary excretion. Although [^{18}F]FAMT has been reported as a LAT1-specific substrate, its rapid washout remains a limitation for static PET imaging. By contrast, [^{18}F]FAMT-OMe demonstrated significantly higher tumor uptake on PET compared with [^{18}F]FAMT, indicating its potential as a promising LAT1-targeted PET probe.

In this study, both tracers of [^{18}F]FAMT-OMe and [^{18}F]FAMT were successfully obtained in a radiochemical yield of approximately 10% with enantiomeric purity greater than 90% using novel precursors bearing mono-Boc and tert-butyl protecting groups. However, Hamacher et.al and Tredwell et al. have previously reported that the introduction of trityl or di-Boc group, rather than mono-Boc, can provide higher enantiomeric purity and improved ^{18}F-labeling efficiency. In the present work, we selected the mono-Boc strategy because of its synthetic simplicity. Nevertheless, as this agent moves closer to potential clinical application, we plan to further optimize the protecting groups to achieve higher yields and improved product quality. In addition, we intend to establish appropriate quality specifications to ensure suitability for intravenous administration in humans, including evaluation of residual copper ions in the final formulation, which was not assessed in the current study [10,11].

OAT1 is responsible for transporting hydrophobic substrates with partial negative charges from the blood into renal proximal tubule cells, facilitating drug excretion [5]. In this study, we evaluated the biodistribution and tumor uptake of [^{18}F]FAMT-OMe, in which the hydroxyl functional group (-OH) was substituted with a methoxy functional group (-O-CH_3) at the 4th carbon position of [^{18}F]FAMT, to reduce the interaction of the PET probe with OAT1 in the kidney.

To confirm the high specificity of [^{18}F]FAMT-OMe for LAT1, attributed to the presence of its alpha-methyl moiety, we conducted both in vitro and in vivo experiments using LAT1 inhibitors, which block the transport of essential amino acids into cancer cells [12]. In this study, BCH and Nanvuranlat were employed as LAT1 inhibitors to suppress LAT1-mediated uptake prior to radiopharmaceutical administration. BCH acts as a system L inhibitor, affecting both LAT1 and LAT2 transporters, resulting in low selectivity toward LAT1 [13–16]. In contrast, several studies have reported that Nanvuranlat is a promising LAT1 inhibitor with higher selectivity for LAT1. Oda et al. demonstrated that Nanvuranlat inhibits LAT1-expressing cells with minimal effects on

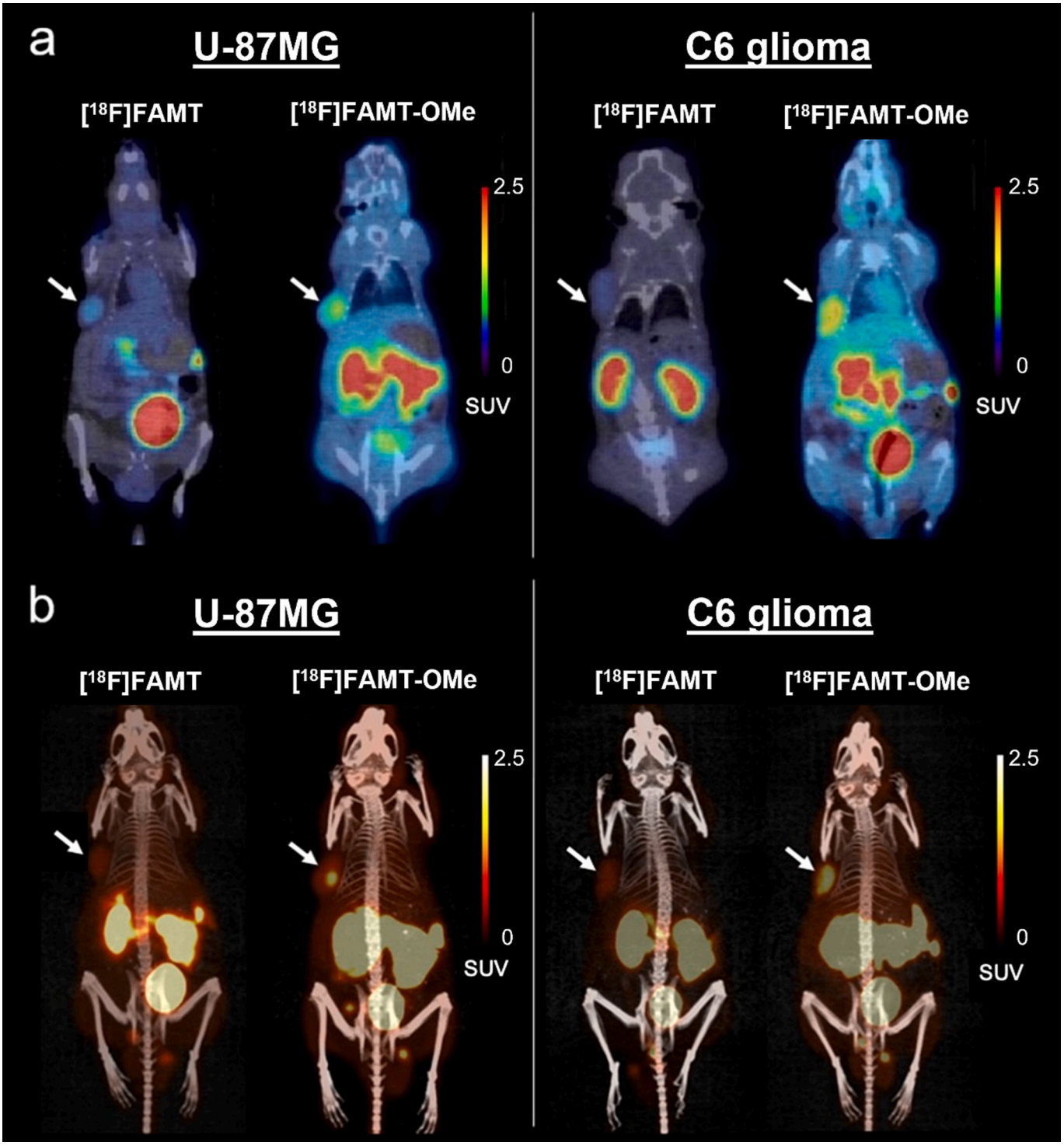

Fig. 3. Representative positron-emission tomography/computed tomography (PET/CT) images of [^{18}F]FAMT-OMe and [^{18}F]FAMT PET at 60-min post-injection in C6 glioma and U-87MG xenograft mice: (a) Coronal view and (b) maximum intensity projection of PET/CT fusion images (arrows indicate tumors).

LAT2-expressing cells. This selective inhibition may reduce off-target effects in LAT1-specific radiopharmaceutical applications [13]. The high selectivity of Nanvuranlat is particularly advantageous for studies involving LAT1-specific radiopharmaceuticals, such as FAMT and IMT, which also contain an alpha-methyl moiety [17–21].

For in vitro analyses using HEK293 and LAT1/HEK293 cells, uptake of [^{18}F]FAMT-OMe was significantly lower in LAT1/HEK293 cells treated with BCH or Nanvuranlat at 0.5, 1, 5, and 10 min post-incubation compared with the control group, indicating a substantial contribution of LAT1 to radiotracer uptake (Fig. 2b). Uptake was also significantly suppressed by BCH and Nanvuranlat in C6 glioma and U-87MG cells, indicating that uptake in these tumors was predominantly LAT1-mediated (Fig. 2c). In in vivo PET experiments, the dynamic uptake curve of [^{18}F]FAMT-OMe in C6 glioma tumors revealed higher uptake in the control group than in the BCH- and Nanvuranlat-treated groups, persisting up to 60 min post-injection (Fig. 7b). Static PET analysis further demonstrated higher SUVmean values of [^{18}F]FAMT-OMe in the control group compared with the LAT1-inhibitor-treated

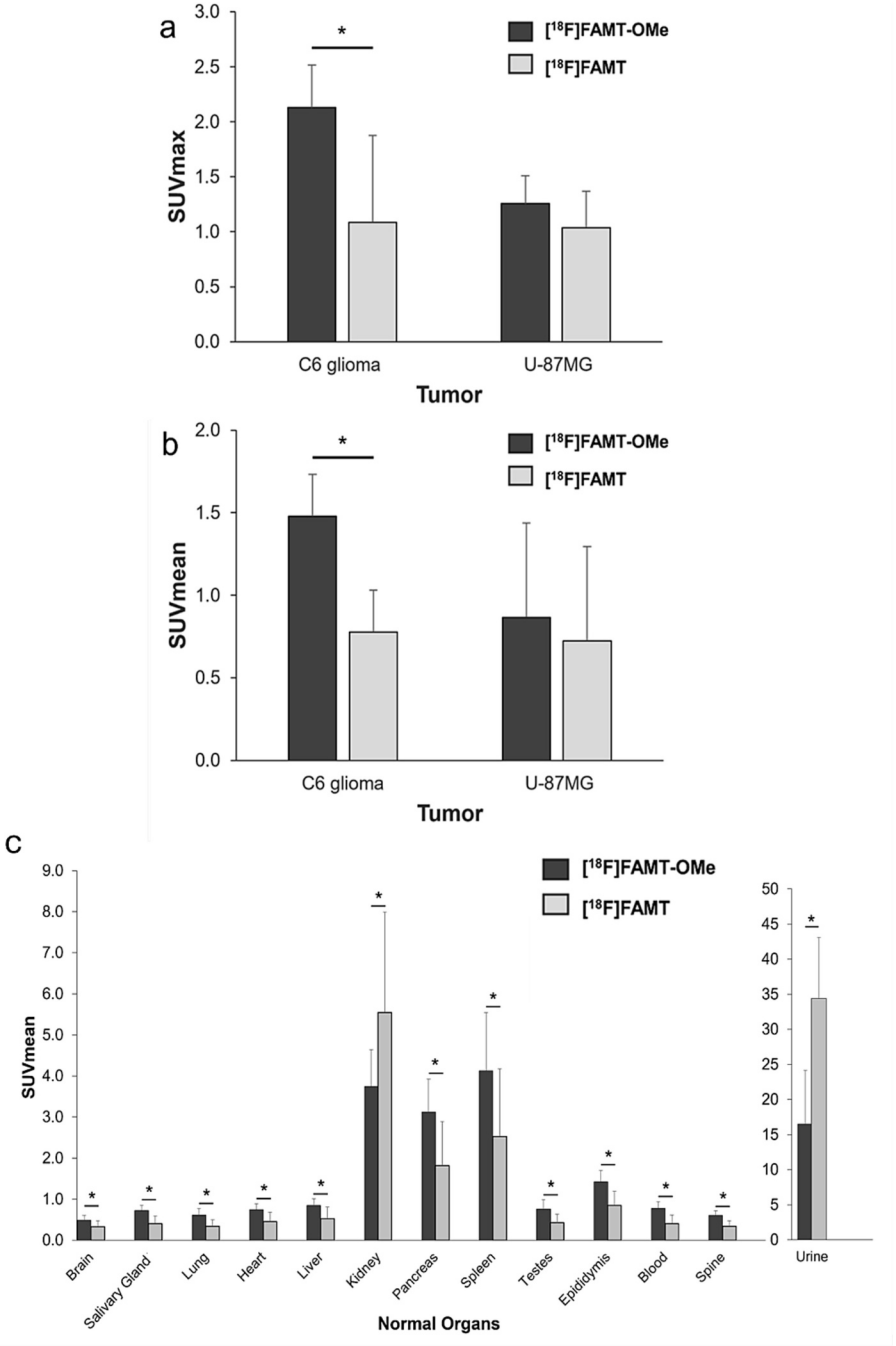

Fig. 4. Comparison of (a) SUVmax and (b) SUVmean between [^{18}F]FAMT-OMe and [^{18}F]FAMT PET in C6 glioma and U-87MG tumor (*P < 0.05) (c) comparison of SUVmean between [^{18}F]FAMT-OMe and [^{18}F]FAMT-OMe. The SUVmean of kidney and urine showed lower uptake on [^{18}F]FAMT-OMe PET than on [^{18}F]FAMT PET (*P < 0.05).

groups in both the C6 glioma tumor and the urine (Fig. 7c). These findings indicate that LAT1 inhibition by BCH or Nanvuranlat reduces [^{18}F]FAMT-OMe uptake in C6 glioma tumors, supporting the conclusion that [^{18}F]FAMT-OMe is predominantly transported via LAT1 expressed on tumor cells.

The uptake of [^{18}F]FAMT-OMe was higher than that of [^{18}F]FAMT in both C6 glioma and U-87MG cells in vitro (Fig. 2a). Although differences in uptake between C6 glioma and U-87MG cells were not pronounced, C6 glioma cells exhibited slightly higher radiotracer uptake by 10 min of equilibrium compared with U-87MG cells. This observation may be attributed to higher LAT1 expression in C6 glioma cells, as indicated by in vitro blocking studies (Fig. 2c) and immunofluorescence staining reported in a previous study (Supplementary Fig. S8) [22].

In the PET analysis, the dynamic curves of tumor uptake showed that [^{18}F]FAMT-OMe uptake in C6 glioma tumors was higher than that of [^{18}F]FAMT throughout the 60 min post-injection. In contrast, the dynamic curves showed lower renal uptake and urinary excretion of [^{18}F]FAMT-OMe than that of [^{18}F]FAMT. [^{18}F]FAMT-OMe exhibited notably improved tumor retention in C6 glioma tumors, accompanied by reduced kidney uptake and urinary excretion relative to [^{18}F]FAMT. The PET results indicated that substituting the hydroxyl functional group with a methoxy functional group effectively inhibited the interaction of OAT1 with the PET probe in the kidneys. This also enhanced the retention in C6 glioma tumors, possibly due to the increased blood

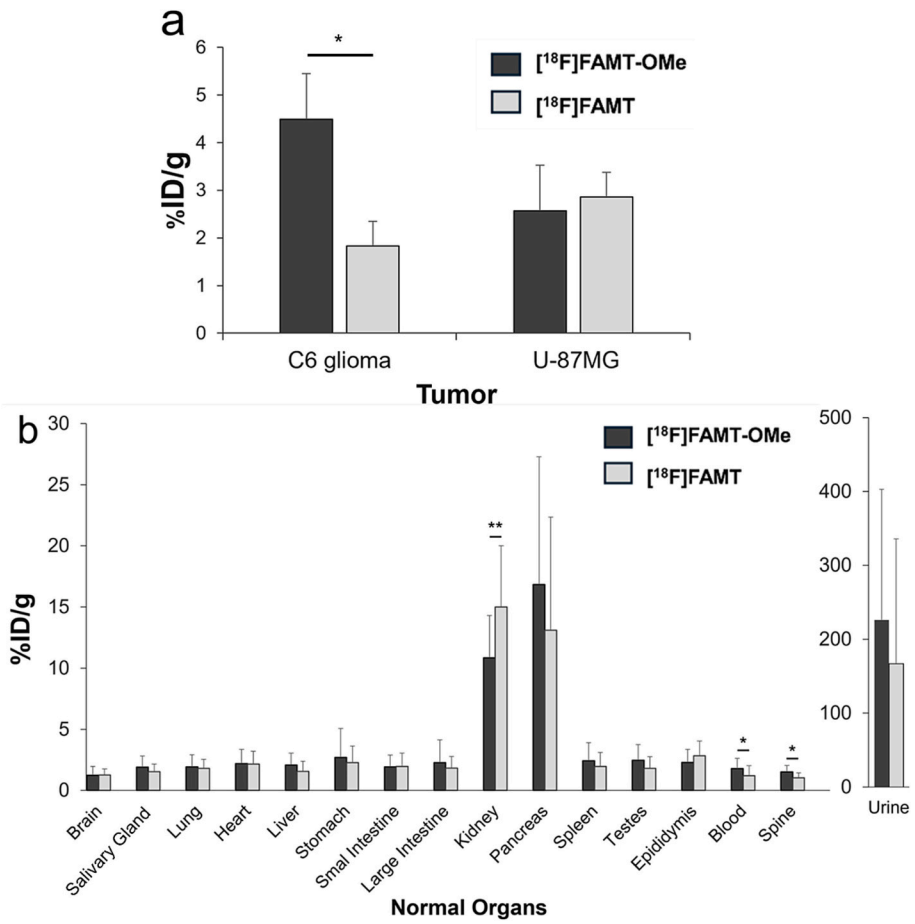

Fig. 5. Comparison of %ID/g. between [^{18}F]FAMT-OMe and [^{18}F]FAMT in (a) C6 glioma and U-87MG tumor and (b) normal organs (*P < 0.05, **P < 0.01).

retention and a greater propensity for tumor uptake compared with [^{18}F]FAMT. However, in U-87MG tumors, the uptake of [^{18}F]FAMT-OMe and [^{18}F]FAMT did not differ significantly. The underlying mechanisms responsible for the differences in uptake between [^{18}F]FAMT-OMe in C6 glioma and U-87MG cells remain unclear. Zheng et al. reported that intra- and intertumoral heterogeneity of LAT1 expression directly impairs selective uptake of LAT1-specific radiotracers like [^{18}F]FBPA, leading to uneven boron delivery and treatment resistance in low LAT1 expression areas [23]. Although a previous study also reported that inhibition of cellular uptake by BCH, an inhibitor of LAT1, was greater in C6 glioma cells than in U-87MG cells. Additional studies to assess the different expression of LAT1 between C6 glioma and U-87MG, for example, immunohistochemistry (IHC) study or Western Blot experiment, is required to clarify LAT1 expression level in both cell lines.

These results suggest that modifying [^{18}F]FAMT by adding a methoxy functional group at the 4th carbon position can successfully decrease its uptake in the kidneys while enhancing its uptake in tumors and increasing blood retention. This was consistent with studies in which probenecid was used to inhibit OAT1 interactions, resulting in reduced accumulation of [^{18}F]FAMT in the kidneys [6]. As shown in Supplementary Data Fig. S9, although the tumor-to-blood ratios (T/B ratios) and tumor-to-muscle ratios (T/M ratios) of [^{18}F]FAMT-OMe in C6 glioma are not significantly different compared with those of [^{18}F]FAMT (T/B ratios: $P = 0.61$, T/M ratios: $P = 0.70$), T/B ratios and T/M ratios of [^{18}F]FAMT are significantly higher in U-87MG tumor (T/B ratios: $P < 0.01$, T/M ratios: $P < 0.05$). These results indicate that [^{18}F]FAMT-OMe not only enhances tumor retention but also prolongs blood retention. However, the increase in blood pool activity of [^{18}F]FAMT-OMe compared with [^{18}F]FAMT is minimal and remained within background levels, which were sufficiently low to allow detection of abnormal tumor uptake.

This study relies primarily on semiquantitative SUV metrics derived from static and dynamic PET imaging. However, full compartmental kinetic modeling experiments to quantify pharmacokinetic parameters were not performed, representing a key limitation. Future investigations incorporating kinetic modeling or transporter saturation studies will be essential to fully characterize the pharmacokinetics and LAT1-specificity of [^{18}F]FAMT-OMe. Furthermore, in-vivo stability of [^{18}F]FAMT-OMe should be performed through metabolite analyses in plasma or urine.

[^{18}F]FAMT is highly specific to LAT1 due to its α-methyl group, which is particularly selective for LAT1 in malignant tumors [13]. Its uptake in non-malignant conditions, such as inflammation or sarcoidosis, is lower, reducing false-positive findings during cancer staging [24]. Since [^{18}F]FAMT-OMe also has an α-methyl group, with sustained selective uptake through LAT1 and better retention in tumors than [^{18}F]FAMT, it may be superior to [^{18}F]FAMT as a PET probe and holds promise for better detection of malignant tumors.

Given the high expression of LAT1 in various malignant tumors and its lower expression in healthy organs, [^{18}F]FAMT-OMe holds potential as a pan-tumor radiopharmaceutical. Therapeutic amino acid derivatives targeting LAT1, such as [^{211}At]AtPA and [^{211}At]AAMT, have been developed [25,26]. These agents could potentially be used to treat various types of cancers with reduced side effects in normal tissues because of the selective LAT1 expression in cancers. However, improving tumor retention is essential to enhance the therapeutic efficacy of LAT1-targeting radioligands that exhibit washout kinetics. A similar approach involves reducing renal uptake and excretion via OAT1 while increasing blood and tumor retention. Although further research

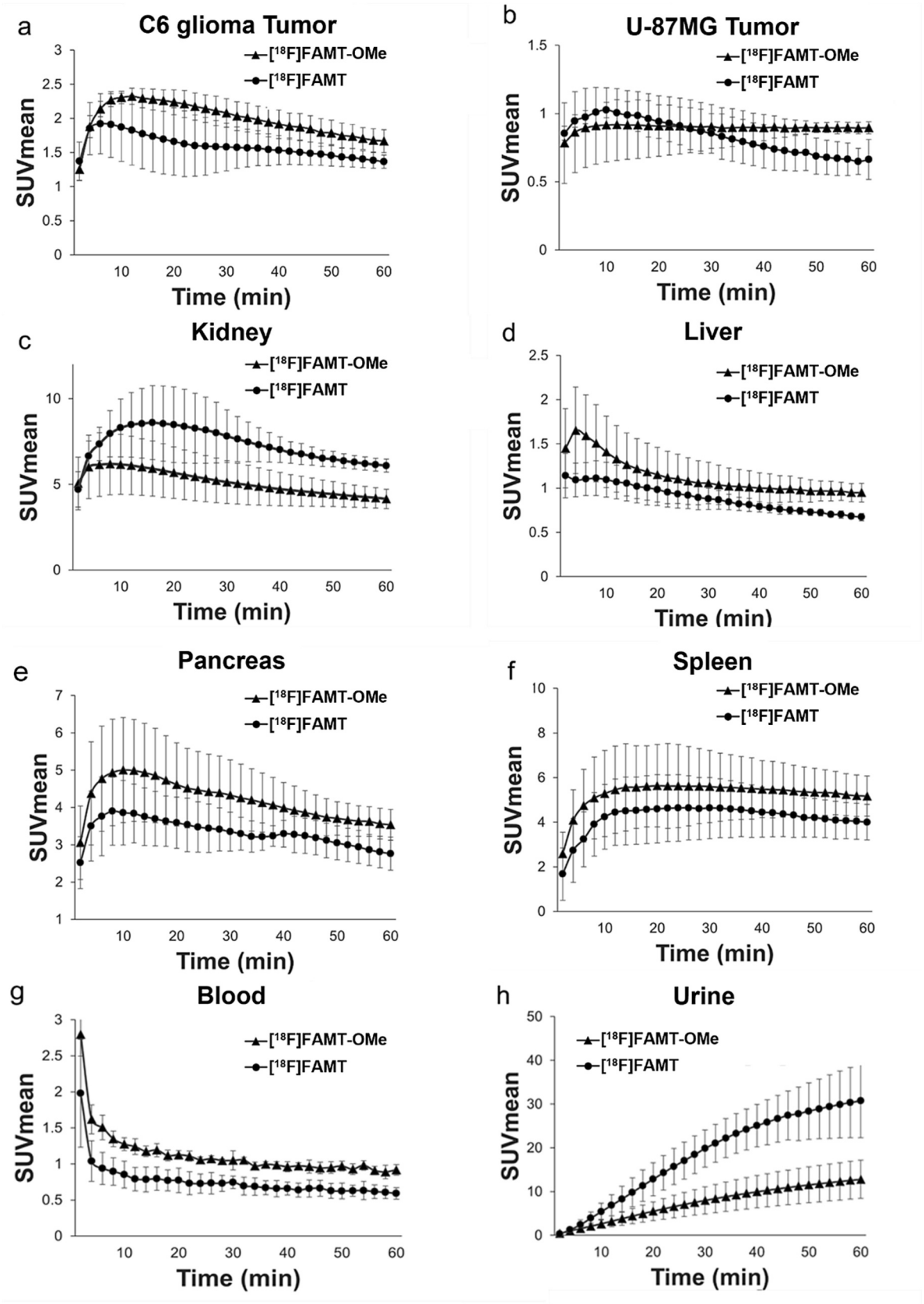

Fig. 6. Dynamic positron-emission tomography curves for the comparison between [^{18}F]FAMT-OMe and [^{18}F]FAMT in (a) C6 glioma tumor, (b) U-87MG tumor, (c) kidney, (d) liver, (e) pancreas, (f) spleen, (g) blood, and (h) urine. Data are expressed as mean ± standard deviation.

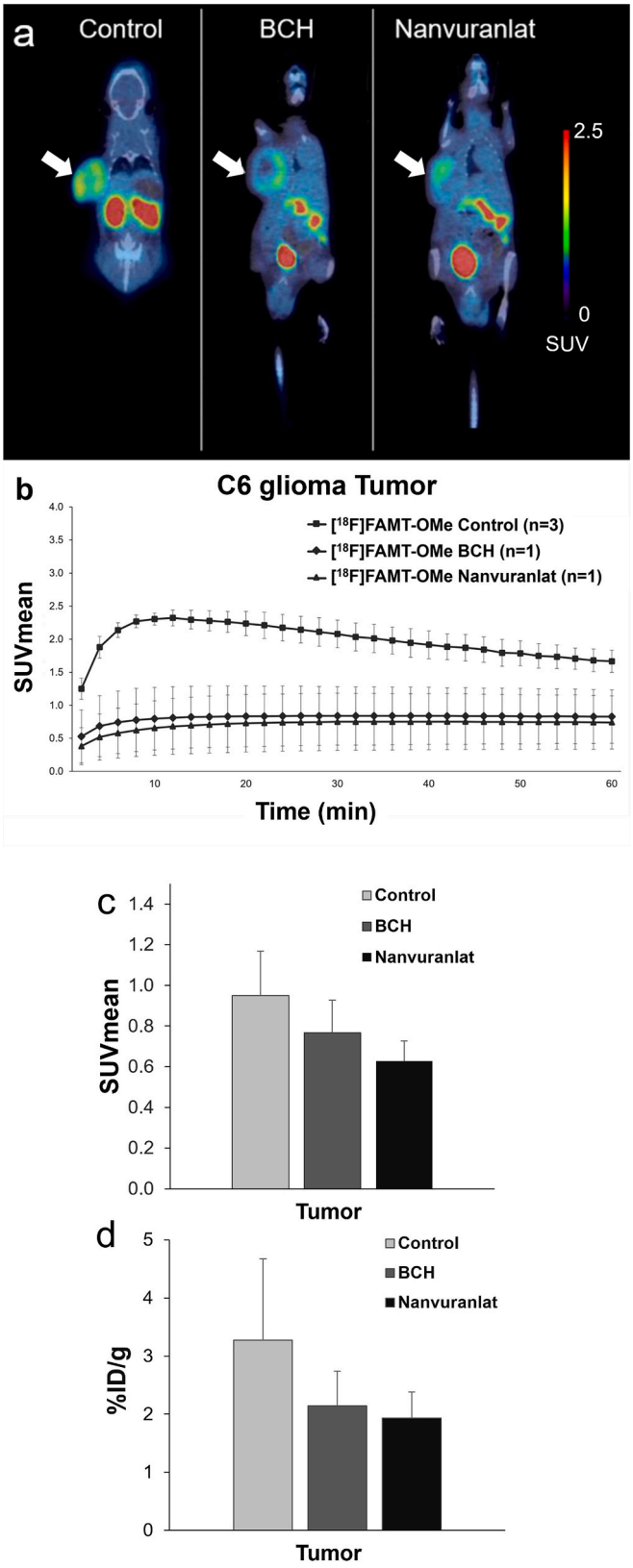

Fig. 7. (a) Coronal view of PET/CT fusion images of [^{18}F]FAMT-OMe at 60-min post-injection in C6 glioma xenograft mice pretreated with BCH or Nanvuranlat (arrows indicate tumors). (b) Dynamic curves of SUVmean of [^{18}F]FAMT-OMe after injection of LAT1 inhibitors (BCH or Nanvuranlat) in C6 glioma tumors. (c, d) SUVmean and %ID/g of [^{18}F]FAMT-OMe in C6 glioma tumors at 1 h post-injection following pretreatment with the LAT1 inhibitors (BCH (n = 3) or Nanvuranlat (n = 3)).

is necessary to investigate the diagnostic and therapeutic efficacies of [^{18}F]FAMT-OMe which is expected to serve as a companion diagnostic PET probe and as a potential compound for optimizing therapeutic radioligands in the future research.

This study had some limitations. First, we evaluated only two types of brain tumor models; therefore, future studies should assess other types of tumor-bearing models. Second, the selectivity for LAT1 was not fully evaluated in this study. More detailed studies are needed to determine the Michaelis–Menten constant and to conduct in vitro evaluations using LAT1-expressing cells. Third, static PET and dynamic PET were performed up to 60 min after injection with small sample size of dynamic PET which may not reflect the biodistribution of the radiotracer after PET acquisition. Delayed PET imaging at 3–4 h post-injection, after recovery from anesthesia, would provide a more accurate characterization of long-term tumor retention and background clearance as well as increasing the sample size. Fourth, the PET studies were primarily conducted in semiquantitative SUV metrics. Further studies, for example, kinetic modeling study to clarify pharmacokinetic information with quantitative parameters of the radiotracer, and immunohistochemistry (IHC) study or Western Blot experiment to investigate the expression level of LAT1 in each type of tumor should be performed. Finally, the clinical utility of [^{18}F]FAMT-OMe PET remains to be confirmed. We have already conducted clinical research using the LAT1-selective probe [^{18}F]FBPA in lung cancers and mediastinal tumors and have obtained a clinical proof-of-concept [4]. Future clinical translation of [^{18}F]FAMT-OMe PET is necessary to evaluate its usefulness in oncology patients, including comparative studies with other LAT1-targeting PET probes.

5. Conclusion

This study demonstrated that the novel PET radiotracer [^{18}F]FAMT-OMe exhibits improved tumor retention compared with [^{18}F]FAMT in a C6 glioma model, along with prolonged blood retention and significantly reduced renal uptake and urinary excretion, suggesting its potential for improved tumor detection.

CRediT authorship contribution statement

Thosapol Sampunta: Writing – review & editing, Writing – original draft, Methodology, Investigation, Formal analysis, Data curation. **Tadashi Watabe:** Writing – review & editing, Supervision, Methodology, Investigation, Funding acquisition, Conceptualization. **Sadahiro Naka:** Writing – review & editing, Methodology, Investigation, Conceptualization. **Kazuko Kaneda-Nakashima:** Writing – review & editing, Methodology, Investigation. **Yoichiro Ohta:** Writing – review & editing. **Takanori Kobayashi:** Writing – review & editing, Investigation, Formal analysis. **Kenta Kurimoto:** Writing – review & editing, Investigation. **Kayako Isohashi:** Writing – review & editing. **Mitsuaki Tatsumi:** Writing – review & editing. **Hiroki Kato:** Writing – review & editing. **Yoshikatsu Kanai:** Writing – review & editing. **Mitsunori Kirihata:** Writing – review & editing. **Noriyuki Tomiyama:** Writing – review & editing.

Consent for publication

Not applicable.

Ethics approval

All animal experiments were performed in compliance with the guidelines of the Institute of Experimental Animal Sciences. The protocol was approved by the Animal Care and Use Committee of Osaka University Graduate School of Medicine (approval number: 05-049-000).

Funding

This study was funded by the KAKENHI Grant-in-Aid for Scientific Research (C) (grant number: 17K10362) and the commissioned research fund provided by F-REI (JPFR25040302).

Declaration of competing interest

The authors have no relevant financial or non-financial interests to disclose.

Acknowledgments

We thank Rumi Saika and the SAS staff for their excellent technical assistance.

This research was performed by the commissioned research fund provided by F-REI (JPFR25040302).

Appendix A. Supplementary data

Supplementary data to this article can be found online at https://doi.org/10.1016/j.nucmedbio.2026.109623.

Data availability

The datasets supporting the conclusions of this article are included within the article and its additional file.

References

[1] Gillies RJ, Robey I, Gatenby RA. Causes and consequences of increased glucose metabolism of cancers. J Nucl Med 2008;49(Suppl. 2):24S–42S. https://doi.org/10.2967/jnumed.107.047258.

[2] Wiriyasermkul P, Nagamori S, Tominaga H, Oriuchi N, Kaira K, Nakao H, et al. Transport of 3-fluoro-L-α-methyl-tyrosine by tumor-upregulated L-type amino acid transporter 1: a cause of the tumor uptake in PET. J Nucl Med 2012;53:1253–61. https://doi.org/10.2967/jnumed.112.103069.

[3] Zhao Y, Wang L, Pan J. The role of L-type amino acid transporter 1 in human tumors. Intractable Rare Dis Res 2015;4:165–9. https://doi.org/10.5582/irdr.2015.01024.

[4] Watabe T, Ose N, Naka S, Fukui E, Kimura T, Kanou T, et al. Evaluation of LAT1 expression in patients with lung cancer and mediastinal tumors: 18F-FBPA PET study with immunohistological comparison. Clin Nucl Med 2023;48:853–60. https://doi.org/10.1097/RLU.0000000000004816.

[5] Jin C, Wei L, Ohgaki R, Tominaga H, Xu M, Okuda S, et al. Interaction of halogenated tyrosine/phenylalanine derivatives with organic anion transporter 1 in the renal handling of tumor imaging probes. J Pharmacol Exp Ther 2020;375:451–62. https://doi.org/10.1124/jpet.120.000235.

[6] Kanai A, Hanaoka H, Yamaguchi A, Mahendra I, Palangka C, Ohshima Y, et al. Enhancing the accumulation level of 3-[^{18}F]fluoro-L-α-methyltyrosine in tumors by preloading probenecid. Nucl Med Biol 2022;104–105:47–52. https://doi.org/10.1016/j.nucmedbio.2021.11.006.

[7] Wei L, Tominaga H, Ohgaki R, Wiriyasermkul P, Hagiwara K, Okuda S, et al. Transport of 3-fluoro-L-α-methyl-tyrosine (FAMT) by organic ion transporters explains renal background in [18F]FAMT positron emission tomography. J Pharmacol Sci 2016;130:101–9. https://doi.org/10.1016/j.jphs.2016.01.001.

[8] Nakajima S, Shikano N, Kotani T, Ogura M, Nishii R, Yoshimoto M, et al. Pharmacokinetics of 3-[125I]iodo-alpha-methyl-L-tyrosine, a tumor imaging agent, after probenecid loading in mice implanted with colon cancer DLD-1 cells. Nucl Med Biol 2007;34:1003–8. https://doi.org/10.1016/j.nucmedbio.2007.06.017.

[9] Khunweeraphong N, Nagamori S, Wiriyasermkul P, Nishinaka Y, Wongthai P, Ohgaki R, et al. Establishment of stable cell lines with high expression of heterodimers of human 4F2hc and human amino acid transporter LAT1 or LAT2 and delineation of their differential interaction with α-alkyl moieties. J Pharmacol Sci 2012;119(4):368–80. https://doi.org/10.1254/jphs.12124fp.

[10] Hamacher K, Coenen HH. Efficient routine production of the 18F-labelled amino acid O-2-18F fluoroethyl-L-tyrosine. Appl Radiat Isot Incl Data Inst Methods Use Agric Ind Med 2002;57(6):853–6. https://doi.org/10.1016/s0969-8043(02)00225-7.

[11] Tredwell M, Preshlock SM, Taylor NJ, Gruber S, Huiban M, Passchier J, et al. A general copper-mediated nucleophilic ^{18}F fluorination of arenes. Angew Chem Int Ed Engl 2014;53(30):7751–5. https://doi.org/10.1002/anie.201404436.

[12] Shi Z, Kaneda-Nakashima K, Ohgaki R, Xu M, Okanishi H, Endou H, et al. Inhibition of cancer-type amino acid transporter LAT1 suppresses B16-F10 melanoma metastasis in mouse models. Sci Rep Aug 25 2023;13(1):13943. https://doi.org/10.1038/s41598-023-41096-3.

[13] Oda K, Hosoda N, Endo H, Saito K, Tsujihara K, Yamamura M, et al. L-type amino acid transporter 1 inhibitors inhibit tumor cell growth. Cancer Sci 2010;101(1):173–9. https://doi.org/10.1111/j.1349-7006.2009.01386.x.

[14] Kanai Y, Segawa H, Miyamoto Ki, Uchino H, Takeda E, Endou H. Expression cloning and characterization of a transporter for large neutral amino acids activated by the heavy chain of 4F2 antigen (CD98). J Biol Chem 1998;273(37):23629–32. https://doi.org/10.1074/jbc.273.37.23629.

[15] Kanai Y. Amino acid transporter LAT1 (SLC7A5) as a molecular target for cancer diagnosis and therapeutics. Pharmacol Ther 2022;230:107964. https://doi.org/10.1016/j.pharmthera.2021.107964.

[16] Bodoy S, Martín L, Zorzano A, Palacín M, Estévez R, Bertran J. Identification of LAT4, a novel amino acid transporter with system L activity. J Biol Chem 2005;280(12):12002–11. https://doi.org/10.1074/jbc.M408638200.

[17] Segawa H, Fukasawa Y, Miyamoto K, Takeda E, Endou H, Kanai Y. Identification and functional characterization of a Na+-independent neutral amino acid transporter with broad substrate selectivity. J Biol Chem 1999;274(28):19745–51. https://doi.org/10.1074/jbc.274.28.19745.

[18] Shikano N, Kanai Y, Kawai K, Inatomi J, Kim DK, Ishikawa N, et al. Isoform selectivity of 3-125I-iodo-alpha-methyl-L-tyrosine membrane transport in human L-type amino acid transporters. J Nucl Med 2003;44(2):244–6.

[19] Wagner CA, Lang F, Bröer S. Function and structure of heterodimeric amino acid transporters. Am J Physiol Cell Physiol 2001;281(4):C1077–93. https://doi.org/10.1152/ajpcell.2001.281.4.C1077.

[20] Nobusawa A, Kim M, Kaira K, Miyashita G, Negishi A, Oriuchi N, et al. Diagnostic usefulness of ^{18}F-FAMT PET and L-type amino acid transporter 1 (LAT1) expression in oral squamous cell carcinoma. Eur J Nucl Med Mol Imaging 2013;40(11):1692–700. https://doi.org/10.1007/s00259-013-2477-9.

[21] Utsugi T, Shibata J, Sugimoto Y, Aoyagi K, Wierzba K, Kobunai T, et al. Antitumor activity of a novel podophyllotoxin derivative (TOP-53) against lung cancer and lung metastatic cancer. Cancer Res 1996;56(12):2809–14.

[22] Aoki M, Watabe T, Nagamori S, Naka S, Ikeda H, Kongpracha P, et al. Distribution of LAT1-targeting PET tracer was independent of the tumor blood flow in rat xenograft models of C6 glioma and MIA PaCa-2. Ann Nucl Med 2019;33:394–403. https://doi.org/10.1007/s12149-019-01346-9.

[23] Zheng X, Pan J, Lin D, Shao W. L-type amino acid transporter 1 in enhancing boron neutron capture therapy: mechanisms, challenges and future directions (review). Int J Mol Med 2025;56(5):170. https://doi.org/10.3892/ijmm.2025.5611.

[24] Kaira K, Oriuchi N, Otani Y, Yanagitani N, Sunaga N, Hisada T, et al. Diagnostic usefulness of fluorine-18-alpha-methyltyrosine positron emission tomography in combination with 18F-fluorodeoxyglucose in sarcoidosis patients. Chest 2007;131:1019–27. https://doi.org/10.1378/chest.06-2160.

[25] Watabe T, Kaneda-Nakashima K, Shirakami Y, Liu Y, Ooe K, Teramoto T, et al. Targeted alpha therapy using astatine (^{211}At)-labeled phenylalanine: a preclinical study in glioma bearing mice. Oncotarget 2020;11:1388–98. https://doi.org/10.18632/oncotarget.27552.

[26] Kaneda-Nakashima K, Zhang Z, Manabe Y, Shimoyama A, Kabayama K, Watabe T, et al. α-Emitting cancer therapy using ^{211} At-AAMT targeting LAT1. Cancer Sci 2021;112:1132–40. https://doi.org/10.1111/cas.14761.